Dalton Transactions

Cite this: *Dalton Trans.*, 2012, **41**, 9192

www.rsc.org/dalton

PAPER

Synthesis, characterisation and antitubercular activities of a series of pyruvate-containing aroylhydrazones and their Cu-complexes†

Abeda Jamadar,[a] Anne-K. Duhme-Klair,*[a] Kiranmayi Vemuri,[b] Manjula Sritharan,*[b] Prasad Dandawate[c] and Subhash Padhye*[c]

Received 13th February 2012, Accepted 17th May 2012
DOI: 10.1039/c2dt30322a

A series of eight pyruvate-based aroylhydrazones was synthesised and characterised. The reaction of the sodium salts of the aroylhydrazones with one equivalent of copper(II) chloride allowed the isolation of neutral 1 : 1 complexes in which the hydrazones occupy three basal coordination sites of a square pyramidal Cu(II)-centre, with two solvent molecules completing the coordination sphere. Structural details were obtained through the determination of the crystal structures of two representative pyruvate-based aroylhydrazones and three Cu(II) complexes. The evaluation of the antimycobacterial activity of the sodium salts of the eight pryruvate hydrazones showed that the compounds are essentially inactive in their anionic form. The corresponding neutral Cu(II) complexes, however, exhibit promising antimycobacterial activities if tested under high iron (8 μg Fe per mL) conditions. As observed for the related antimycobacterial agent isoniazid, the activity of the complexes decreases if the *M. tuberculosis* cells are grown under low iron (0.02 μg Fe per mL) conditions. The Cu(II) complexes may thus have a similar mode of action and may require an iron-containing heme-dependent peroxidase for activation.

Introduction

Tuberculosis (TB) is a highly infectious airborne disease caused by the pathogenic bacterium *Mycobacterium tuberculosis*. It is estimated that TB affects approximately one third of the world's population.[1] Whilst the antitubercular drugs that are presently available for treatment are effective against actively growing drug-susceptible bacteria, they often fail to eradicate resistant and persistent strains.[2,3]

In the search for new antitubercular agents with improved efficacy, a variety of substituted acyl hydrazones (Scheme 1) derived from the front-line antitubercular agents isoniazid (isonicotinyl hydrazide, INH, R′ = 4-pyridyl) and pyrazinamide (PZA, R′ = 2-pyrazinyl) have been investigated for their activity against *M. tuberculosis*.[4–9] The most promising strategies in the design of INH-based hydrazones aim to improve the potency of the parent antimicrobial agent by increasing its bioavailabilty. Approaches include the enhancement of the diffusion of the drug through the waxy mycobacterial cell wall by introducing hydrophobic substituents[4,5,10] and the prevention of metabolic acetylation of INH by protecting the free amino group through hydrazone formation.[6,11] INH acetylation is catalysed by both mammalian and mycobacterial *N*-arylaminoacetyl transferases (NATs) and leads to drug deactivation.[12,13]

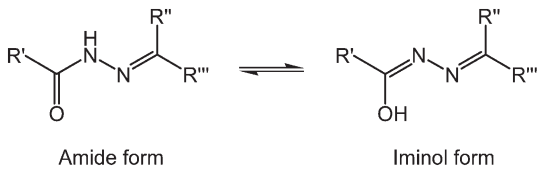

Scheme 1 General structure of acyl hydrazones and their iminol tautomers.

In addition, metal-bound hydrazone derivatives of INH have been reported to possess excellent *in vitro* antimycobacterial activities,[14–16] with some complexes even retaining activity against resistant strains.[17] It is well established that acyl hydrazones form stable chelate complexes with transition metal cations by utilising both their oxygen and imine nitrogen as donor atoms.[14,18] Importantly, acyl hydrazones allow additional donor sites to be introduced (*via* R″ and R‴, Scheme 1) in order to increase the denticity of the resulting ligands and hence their affinity for biologically relevant metal ions, such as Cu(II), Mn(II) and Fe(II).[19–21]

A factor that may contribute to the observed enhanced antimycobacterial activity of metal-bound acyl hydrazones is that metal coordination to the deprotonated anionic form of the

[a]*Department of Chemistry, University of York, Heslington, York YO10 5DD, UK. E-mail: anne.duhme-klair@york.ac.uk; Fax: (+44) (0)1904 322516*
[b]*Department of Animal Sciences, School of Life Sciences, University of Hyderabad, Hyderabad 500046, India. E-mail: srimanju@yahoo.com; Fax: (+91) 40 23010307*
[c]*ISTRA, Department of Chemistry, Abeda Inamdar College, University of Pune, Pune 411001, India. E-mail: sbpadhye@hotmail.com; Fax: (+91) 20 26446970*

† Electronic supplementary information (ESI) available. CCDC reference numbers 866682 & 866686. For ESI and crystallographic data in CIF or other electronic format see DOI: 10.1039/c2dt30322a

ligand can give rise to neutral complexes with enhanced lipophilicity, thus facilitating drug transport through the mycobacterial cell wall.[14,16] Since certain mycobacterial resistance mechanisms are modulated by intracellular oxidative stress[22] the redox activity of the metal centres in metallodrugs of this type may be significant. Free intracellular Cu(I) or Fe(II) cations, for example, cause oxidative stress, which in turn initiates the expression of the catalase-peroxidase KatG[23] involved in the activation of the antitubercular prodrug INH. One of us (M. S.) has previously shown that the effectiveness of INH is associated with the iron status of the organisms since the peroxidase activity required for activation of INH is considerably lowered upon iron deficiency. In contrast, iron-sufficient *M. tuberculosis* cells showing notable peroxidase activity are susceptible to INH treatment.[24,25] Recently it was also reported that *M. tuberculosis* is more susceptible to the toxicity of free copper than other bacteria and it was suggested that the mammalian immune system utilizes Cu(I) as a defense mechanism against *M. tuberculosis*.[26]

By considering the factors discussed above, we have designed a series of aroyl hydrazones and their Cu complexes (Scheme 2). In order to gain an element of diversity, the intensely studied INH framework was replaced with a series of mono- and di-substituted aroyl analogues. Our decision to move away from the INH framework was encouraged by recent reports that confirm that hydrazones derived from fluoro-, chloro- and nitrobenzoyl hydrazides or even benzoyl hydrazide can exhibit promising antimycobacterial activities.[27,28] The finding that benzoyl hydrazide forms an NAD adduct similar to the INH-NAD adduct responsible for the antitubercular activity of INH suggests that benzoyl hydrazide may have the same mode of action.[29] We anticipate that upon removal of the Cu-centre from the ligands, for example due to Cu-sequestration by mycobacterial metallothionein,[26] the hydrazone ligands are released and subsequently hydrolyse to give their respective parent hydrazides and pyruvate. Antitubercular activity then arises from a combination of the activity of the parent hydrazide and copper toxicity. In addition, the hydrazide–hydrazone derived from pyrazinoic acid was investigated. Pyrazinoic acid is of particular interest since this hydrolysis product of the antitubercular agent pyrazinamide is able to target persisting *M. tuberculosis*. Only very recently, pyrazinoic acid was found to inhibit trans-translation, a process important in stress survival and recovery from nutrient starvation.[30]

The pyruvate moiety was introduced in order to prevent metabolic acetylation of the parent hydrazides and to provide an additional oxygen donor for copper binding. Since the pyruvate moiety is deprotonated at physiological pH, it balances a positive charge of the bound metal cations and thus allows the preparation of neutral complexes to facilitate diffusion into the mycobacterial cell. In addition, a recent computational study showed that pyruvate-based hydrazones can bind to and potentially inhibit the active site of isocitrate lyase (ICL).[31] Since ICL plays a crucial role in the persistence of *M. tuberculosis*, it is considered an attractive target for novel antitubercular drugs.[32] The docking study found that the binding affinities of the pyruvate hydrazones investigated were comparable to the affinity obtained for pyruvate. The higher binding affinity obtained for some of the hydrazone ligands may be due to additional hydrogen bond formation by nitrogen atom.[21] Hence, combining

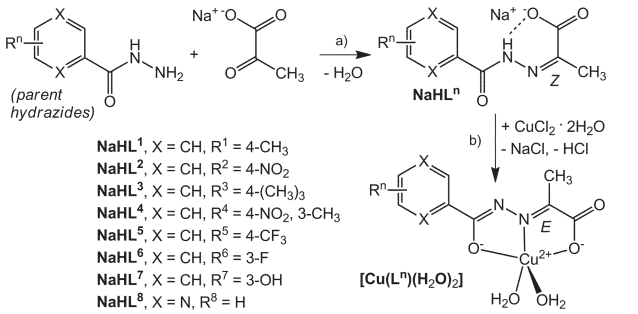

Scheme 2 Preparation of pyruvate-based hydrazones **NaHL^1**–**NaHL^8** and their copper(II) complexes [Cu(**L^1**)$(H_2O)_2$]–[Cu(**L^8**)$(H_2O)_2$]. Conditions: (a) methanol–water (7 : 3), reflux for 2 h; (b) methanol, 25 °C, 2 h.

pyruvate with isoniazid-analogues and binding the resulting hydrazones to Cu(II) may result in prodrugs that after activation do not only kill actively growing bacteria but also show activity against persistent strains.

Within this study, a total of eight pyruvate hydrazones and their Cu(II)-complexes were synthesised, characterised and tested against *M. tuberculosis* grown initially in Middlebrook 7H9 medium and then compounds exhibiting low MIC values were screened under high (8 μg Fe per mL) and low (0.02 μg Fe per mL) iron conditions.

Results and discussion

Synthesis and characterisation

The pyruvate-based hydrazone salts **NaHL^1**–**NaHL^8** were synthesised in good yields by Schiff base condensation of commercially available hydrazides with sodium pyruvate (Scheme 2). After recrystallisation from ethanol, **NaHL^1**–**NaHL^8** were obtained as white to pale yellow powders and characterized by IR, ^{1}H and ^{13}C NMR spectroscopy, mass spectrometry and elemental analysis. Details are given in the ESI.†

Acyl hydrazones can potentially form amide/iminol-tautomers and *E*/*Z*-isomers,[33] as indicated in Schemes 1 and 2, respectively. For biologically active thiosemicarbazones, which share key structural features with acyl hydrazones, detailed recent studies have shown that *E*/*Z* isomerisation and tautomerisation processes affect the metal-chelating properties of these ligands.[34,35]

In order to investigate which *E*/*Z*-isomers and amide/iminol-tautomers are formed by the sodium salts of the acyl hydrazones in the solid state, the crystal structure of **NaHL^1** was determined. Single crystals were obtained by slow evaporation of a concentrated solution of **NaHL^1** in ethanol. Selected bond angles and distances are given in Table 1. As shown in Fig. 1, **NaHL^1** crystallises as the *Z*-isomer and amide-tautomer. The amide hydrogen H(2) could be located in the difference Fourier map. A strong intramolecular hydrogen-bond is formed between H(2) and the deprotonated carboxylate oxygen O(1) of the pyruvate unit ($d_{N(2)–O(1)}$ = 2.5772(14) Å). The C(3)–N(2) bond length of 1.3522(16) Å is consistent with a single bond whilst the hydrazinic C(3)═O(3) bond length of 1.2330(15) Å shows double bond character.[36] However, the similarity of the bond angles at N(1) of

Table 1 Selected bond lengths (Å) and angles (°) for **NaHL**[1] and **H_2L**[8]

NaHL[1]		**H_2L**[8]	
C(1)–O(1)	1.2743(16)	C(7)–O(2)	1.3163(17)
C(1)–O(2)	1.2380(16)	C(7)–O(3)	1.2151(17)
C(3)–O(3)	1.2330(15)	C(5)–O(1)	1.2209(17)
C(2)–N(1)	1.2897(17)	C(6)–N(4)	1.2831(18)
C(3)–N(2)	1.3522(16)	C(5)–N(3)	1.3616(18)
N(1)–N(2)	1.3835(15)	N(3)–N(4)	1.3745(16)
N(1)···O(4)	2.9249(15)	O(2)...O(4)	2.5642(14)
N(2)···O(1)	2.5772(14)		
C(3)–N(2)–N(1)	119.46(11)	C(5)–N(3)–N(4)	117.71(12)
C(2)–N(1)–N(2)	117.29(11)	N(3)–N(4)–C(6)	116.30(12)
Na(1)–O(3)	2.3482(10)		
Na(1)–O(4)	2.3162(11)		
Na(1)–O(5)	2.3952(11)		
Na(1)–O(1)#2	2.4222(11)		
Na(1)–O(4)#1	2.3459(11)		
Na(1)–O(5)#1	2.4232(11)		

Symmetry transformations used to generate equivalent atoms: #1 2/3 − *y*, −2/3 + *x* − *y*, 1/3 + *z*; #2 5/3 − *x*, 1/3 − *y*, 7/3 − *z*.

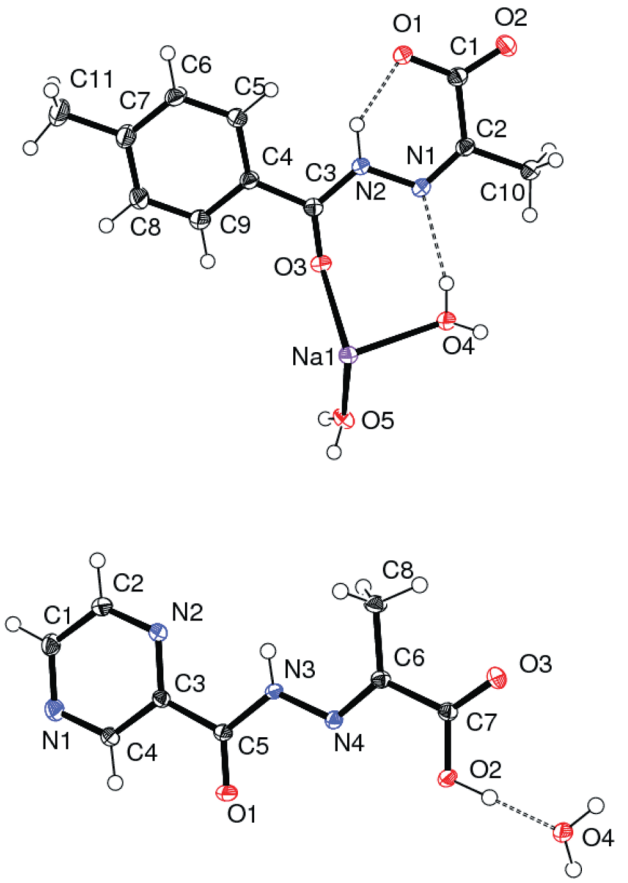

Fig. 1 ORTEP plots (50% probability ellipsoids) of the asymmetric units of **NaHL**[1]·2H_2O (top) and **H_2L**[8]·H_2O (bottom).

117.29(11)° and N(2) of 119.46(11)° indicates the potential for electron delocalisation.

Overall, the bond distances and angles listed in Table 1 are similar to those reported for the protonated neutral pyruvic acid-based hydrazones (H_2L) derived from salicyloyl hydrazide,[37] 4-methylbenzoyl hydrazide[38] and 4-chlorobenzoyl hydrazide.[39] These three neutral pryruvic acid-derivatives crystallise as the *E*-isomers and lack the intramolecular hydrogen bond and sodium counter ion observed in the structure of **NaHL**[1]. In **NaHL**[1] the sodium counter ion interacts with the hydrazinic carbonyl oxygen, thereby slightly lengthening the hydrazinic carbonyl bond. The carboxylate donor of an adjacent symmetry-generated **$HL^{1(1-)}$** anion and four bridging aqua ligands, two of which are symmetry-generated, complete the octahedral coordination sphere of the sodium cation (Fig. S2a and b†).

In order to investigate which isomer is adopted in solution, the ^{1}H NMR spectrum of **NaHL**[1] was recorded immediately after dissolving the solid product in d_6-dmso. The initial spectrum obtained indicated the presence of two species in a 1 : 5.7 ratio (Fig. S1, ESI†). The major species shows a characteristic singlet resonance exceptionally downfield at 16.2 ppm, which could be due to an iminol–OH[40] or a strongly hydrogen-bonded amide proton.[33,35] In view of the strong intramolecular hydrogen bond observed in the crystal structure of **NaHL**[1] the latter seems more likely and is consistent with the amide *Z*-isomer observed in the solid state also dominating in solution. The corresponding amide NH-proton of the minor species is more shielded and resonates at 10.9 ppm, a chemical shift consistent with the NH proton of the *E*-isomer, which lacks intramolecular hydrogen bonding.[33] Upon heating to 378 K, the minor *E*-isomer is readily converted into the more stable *Z*-isomer and remains as such upon subsequent cooling to 298 K. Further support for the assignment of the more stable species as the *Z*-isomer is provided by the ^{13}C NMR data. Palla *et al.*[33] investigated a series of esters of puruvic acid hydrazones and reported that in d_6-dmso a chemical shift of around 20 ppm for the pyruvic methyl carbon is diagnostic for the *Z*-isomer whilst a shift of 13 ppm is characteristic for the *E*-isomer.[37] In the ^{13}C NMR spectra of fully equilibrated solutions of **NaHL**[1]**–NaHL**[8] in d_6-dmso, the pyruvic methyl carbon resonance is observed between 21.1 and 21.6 ppm, further confirming the assignment as *Z*-isomer.

Owing to its relevance to the antitubercular agent pyrazinamide, the crystal structure of the hydrazide–hydrazone derived from pyrazinoic acid was also determined. Crystals of **H_2L**[8] were obtained through evaporation of a slightly acidic solution of the compound in aqueous methanol. The molecular structure of **H_2L**[8] is shown in Fig. 1 and selected bond angles and distances are given in Table 1. Like the neutral pyruvic acid hydrazones reported in the literature,[37–39] **H_2L**[8] adopts the *E*-isomer in the solid state. Again, the amide tautomer is formed with a hydrazinic C(5)═O(1) bond length of 1.2209(17) Å and a C(5)–N(3) bond length of 1.3616(18) Å. The proton on N(3) could be located in the difference Fourier map and O(1) accepts a weak hydrogen bond from an adjacent water molecule ($d_{O(1)–O(4)}$ = 2.9683(16) Å). On the whole, the bond distances and angles are consistent with those reported for other pyruvic acid-based hydrazones.

The copper(II) complexes [Cu(**L^1**)(H_2O)$_2$]–[Cu(**L^8**)(H_2O)$_2$] were prepared by reacting a solution of the respective sodium salts of the ligands in methanol with one equivalent of copper(II) chloride dihydrate. Slow evaporation of the resulting solutions at room temperature yielded green microcrystalline powders, which were purified by washing with water, followed by recrystallisation from methanol. The complexes were obtained in moderate

yields and characterised by IR spectroscopy, mass spectrometry and elemental analysis.

The imine ν(C=N), amide and carboxylato ν(C=O) bands, which are reasonably well resolved in the solid state IR spectra of the free ligands, merge upon complex formation to give a broad band in the range between 1622 and 1649 cm^{-1}. The centre of the broad band is shifted by 10–30 cm^{-1} to lower frequencies if compared with the respective highest frequency ν(C=O) band in the IR spectrum of the free ligand, consistent with a weakening of the bond upon coordination and shift towards the iminolate tautomer.[41]

The positive ion ESI mass spectra of methanolic solutions of complexes [Cu($\mathbf{L^1}$)$(H_2O)_2$]–[Cu($\mathbf{L^8}$)$(H_2O)_2$] are interesting since the observed molecular ion peaks for all but one ([Cu($\mathbf{L^4}$)-$(H_2O)_2$]) of the complexes appear at one m/z unit higher than expected (Fig. S5†). In principle, the higher mass could be explained by either the addition of a hydrogen atom or the addition of a proton with concomitant reduction of Cu(II) to Cu(I) to account for the positive charge. The detection of ions of composition $[M + 2Na]^+$ in the spectra of the copper complexes of $\mathbf{L^1}$, $\mathbf{L^5}$ and $\mathbf{L^6}$ (Fig. S5†) provides support for the latter, as these ions show the addition of a cation which requires the charge to be balanced by a reductive process, most likely the reduction of Cu(II) to Cu(I). The reduction of Cu(II) to Cu(I) in positive ion ESI mass spectra of Schiff base complexes has previously been reported and attributed to the transfer of an electron from a solvent methanol molecule to Cu(II) in the gas phase.[42]

In order to examine the structure of the Cu(II)-complexes formed in more detail, the solid state structures of three representative examples were determined. The ORTEP plot of the asymmetric unit of [Cu($\mathbf{L^1}$)$(H_2O)_2$] is shown in Fig. 2, selected bond lengths and angles are listed in Table 2. The ORTEP plots, selected bond lengths and bond angles for [Cu($\mathbf{L^2}$)$(MeOH)_2$] and [Cu($\mathbf{L^4}$)$(MeOH)_2$] can be found in the ESI (Fig. S3, S4 and Table S1†).

The asymmetric unit obtained for [Cu($\mathbf{L^1}$)$(H_2O)_2$] contains two crystallographically independent complexes with slightly different coordination geometries. Both are square pyramidal, with τ-indices[43] of 0.074 (complex **1**) and 0.125 (complex **2**) indicating that the latter deviates slightly more from perfect square pyramidal geometry. In both complexes, $\mathbf{L^{1(2-)}}$ is doubly deprotonated and acts as a tridentate ligand, forming two 5-membered chelate rings by using the hydrazinic carbonyl oxygen, a pyruvate carboxylate oxygen and the imine nitrogen atom as donors. Two coordinated aqua ligands complete the coordination sphere. Whilst in both complexes, the aqua ligand in apical position is only weakly coordinated, as expected for Jahn–Teller distorted Cu(II) complexes, the apical Cu(1)-O(5) contact of 2.218(2) Å in complex **1** is even longer than the equivalent Cu(2)–O(9) contact of 2.152(2) Å in complex **2**. Whilst the apical aqua ligands hydrogen bond with the pyruvate moieties of adjacent symmetry-generated complexes, each basal aqua ligand donates a hydrogen bond to the hydrazinic carbonyl oxygen of the other complex in the asymmetric unit (Fig. 2).

The bond lengths of the hydrazinic carbonyl groups are 1.301(3) and 1.295(3) Å in complexes **1** and **2**, respectively. Both are slightly longer than the equivalent C(3)–O(3) bond length of 1.2330(15) Å in $\mathbf{NaHL^1}$, however, both still have significant double bond character. Conversely, the C(3)–N(2) and C(14)–N(4) distances of 1.326(3) and 1.328(3) Å in complexes **1** and **2**, respectively, are significantly shorter than the C(3)–N(2) distance of 1.3522(16) Å in $\mathbf{NaHL^1}$. Upon complexation $\mathbf{L^{1(2-)}}$ hence adopts an intermediate structure that lies in between the structures to be expected for the amide and iminol tautomers.

To date, the only other crystal structure of a Cu(II) complex of a pyruvate-based aroylhydrazone that has been deposited in the

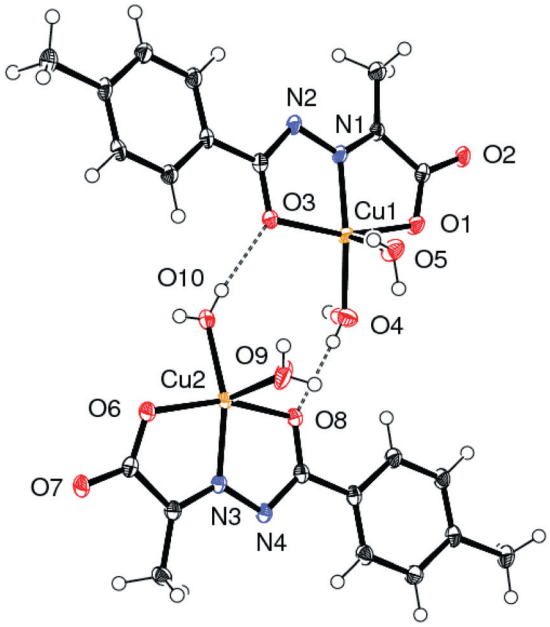

Fig. 2 ORTEP plot (50% probability ellipsoids) of the asymmetric unit of [Cu($\mathbf{L^1}$)$(H_2O)_2$].

Table 2 Selected bond lengths (Å) and angles (°) for [Cu($\mathbf{L^1}$)$(H_2O)_2$]

Complex **1**		Complex **2**	
C(1)–O(1)	1.291(3)	C(12)–O(6)	1.282(3)
C(1)–O(2)	1.226(3)	C(12)–O(7)	1.244(3)
C(3)–O(3)	1.301(3)	C(14)–O(8)	1.295(3)
C(2)–N(1)	1.286(3)	C(13)–N(3)	1.289(3)
C(3)–N(2)	1.326(3)	C(14)–N(4)	1.328(3)
N(1)–N(2)	1.372(2)	N(3)–N(4)	1.371(2)
Cu(1)–N(1)	1.8988(19)	Cu(2)–N(3)	1.9065(19)
Cu(1)–O(4)	1.958(2)	Cu(2)–O(10)	1.971(2)
Cu(1)–O(3)	1.9873(16)	Cu(2)–O(8)	1.9939(16)
Cu(1)–O(1)	1.9877(16)	Cu(2)–O(6)	1.9940(16)
Cu(1)–O(5)	2.218(2)	Cu(2)–O(9)	2.152(2)
N(1)–Cu(1)–O(4)	156.67(9)	N(3)–Cu(2)– (10)	152.75(9)
N(1)–Cu(1)–O(3)	79.98(7)	N(3)–Cu(2)–O(8)	78.91(7)
O(4)–Cu(1)–O(3)	105.71(8)	O(10)–Cu(2)–O(8)	101.09(8)
N(1)–Cu(1)–O(1)	81.46(7)	N(3)–Cu(2)–O(6)	81.66(7)
O(4)–Cu(1)–O(1)	90.13(8)	O(10)–Cu(2)–O(6)	94.46(8)
O(3)–Cu(1)–O(1)	161.11(7)	O(8)–Cu(2)–O(6)	160.22(7)
N(1)–Cu(1)–O(5)	108.83(8)	N(3)–Cu(2)–O(9)	111.51(9)
O(4)–Cu(1)–O(5)	93.73(9)	O(10)–Cu(2)–O(9)	95.72(9)
O(3)–Cu(1)–O(5)	92.16(7)	O(8)–Cu(2)–O(9)	89.83(8)
O(1)–Cu(1)–O(5)	97.10(7)	O(6)–Cu(2)–O(9)	100.79(8)
O(4)···O(8)	2.702(3)	O(10)···O(3)	2.714(3)
O(5)···O(1)#1	2.634(3)	O(9)···O(6)#2	2.778(3)
O(5)···O(7)#2	2.750(2)	O(9)···O(2)#1	2.744(2)

Symmetry transformations used to generate equivalent atoms: #1 $-x + 2, -y + 1, -z + 1$; #2 $-x + 1, -y, -z + 1$.

Cambridge Crystallographic Data Centre (CCDC) is the 1 : 2 complex $[Cu(C_{10}H_9N_2O_4)_2]$ reported by He *et al.* (Fig. 3).[44] In $[Cu(C_{10}H_9N_2O_4)_2]$ the ligand remained mono-protonated. The hydrazinic C=O bond lengths in $[Cu(C_{10}H_9N_2O_4)_2]$ are characteristic of a double bond and resemble those of **NaHL^1**. As expected, the Cu-donor bond distances in the six-coordinate complex $[Cu(C_{10}H_9N_2O_4)_2]$, are slightly longer than those in the five-coordinate complex $[Cu(\mathbf{L^1})(H_2O)_2]$.

Antimycobacterial activity testing

The pyruvate-based hydrazones **NaHL^1**–**NaHL^8**, their parent hydrazides and the copper complexes $[Cu(\mathbf{L^1})(H_2O)_2]$–$[Cu(\mathbf{L^8})(H_2O)_2]$ were screened against *M. tuberculosis* under both low and high iron conditions. INH was used as the reference drug.

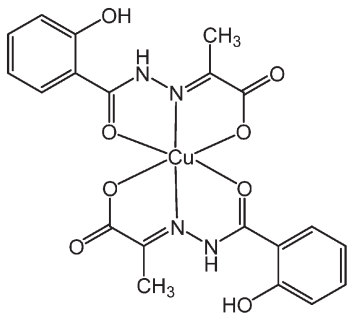

Fig. 3 The 1 : 2 complex $[Cu(C_{10}H_9N_2O_4)_2]$ reported by He *et al.*[44]

Whilst the pyruvate-based hydrazones and their parent hydrazides were found to be inhibitory, their minimum inhibitory concentration (MIC) values were significantly higher than the MIC of INH (Table 3). Once coordinated to Cu(II), however, the pyruvate-based hydrazones were highly potent, with the complexes $[Cu(\mathbf{L^1})(H_2O)_2]$–$[Cu(\mathbf{L^8})(H_2O)_2]$ exhibiting MIC values in the range <0.5–2 μg mL^{-1} when evaluated against *M. tuberculosis* grown under high iron conditions (Table 3). The lower antibacterial activity of the pyruvate-based hydrazones may be rationalised by the fact that they are likely to be anionic at physiological pH (the pK_a value of pyruvic acid is 2.49)[45] and hence less able to diffuse through lipophilic cell membranes. In contrast, the copper(II) complexes under investigation are neutral and may facilitate the cellular uptake of their components. Removal of the copper inside the mycobacterial cell, for example through capture by metallothioneins, could therefore lead to trapping of the hydrophilic hydrazones inside the mycobacterial cell.

If grown under iron-deficient conditions, INH and the complexes $[Cu(\mathbf{L^1})(H_2O)_2]$–$[Cu(\mathbf{L^8})(H_2O)_2]$ were less effective. INH is a prodrug that, upon entry into the pathogen is converted into the active form by KatG, a dual enzyme with catalase and peroxidase activities. The latter, involving an iron-containing heme centre in KatG, is responsible for the generation of free radicals from INH.[46] In earlier studies, one of us (M. S.)[24,25] found a higher MIC (minimum inhibitory concentration) of INH against iron-limited *M. tuberculosis* cells than the routinely used MIC of 0.2 μg mL^{-1} for INH, which applies to higher iron levels in the growth medium. The failure to activate INH under iron-limiting conditions was associated with the low peroxidase activity that was possibly due to decreased heme availability. The observation

Table 3 Influence of iron concentrations in the growth medium on the minimum inhibitory concentrations (MICs) of: (a) INH and $[Cu(\mathbf{L^1})(H_2O)_2]$–$[Cu(\mathbf{L^8})(H_2O)_2]$; (b) **NaHL^1**–**NaHL^8** and their parent hydrazides (low iron: 0.02 μg Fe per mL; high iron: 8 μg Fe per mL, $FeSO_4$ as iron source)

(a)

		MIC of the copper complexes/μg mL^{-1}			
Compound	X, R^n	7H9 medium	High Fe	Low Fe	Fold difference in MIC
INH		0.25	0.125	32	256
$[Cu(\mathbf{L^1})(H_2O)_2]$	CH, 4-Me	4	<0.5	128	>256
$[Cu(\mathbf{L^2})(H_2O)_2]$	CH, 4-NO_2	1	2	256	128
$[Cu(\mathbf{L^3})(H_2O)_2]$	CH, 4-$(CH_3)_3$	4	1	64	64
$[Cu(\mathbf{L^4})(H_2O)_2]$	CH, 4-NO_2, 3-Me	8	<0.5	128	>256
$[Cu(\mathbf{L^5})(H_2O)_2]$	CH, 4-CF_3	8	<0.5	128	>256
$[Cu(\mathbf{L^6})(H_2O)_2]$	CH, 3-F	8	0.5	64	128
$[Cu(\mathbf{L^7})(H_2O)_2]$	CH, 3-OH	16	1	32	32
$[Cu(\mathbf{L^8})(H_2O)_2]$	N, H	4	<0.5	256	>512

(b)

	MIC of the parent hydrazide/μg mL^{-1}			MIC of pyruvate hydrazone ligands/μg mL^{-1}		
Compound	High Fe	Low Fe	Fold difference	High Fe	Low Fe	Fold difference
NaHL^1	32	256	8	16	256	16
NaHL^2	16	256	16	8	256	32
NaHL^3	32	>256	<8	16	256	16
NaHL^4	32	>256	<8	8	128	16
NaHL^5	32	256	8	16	256	16
NaHL^6	64	256	4	16	256	16
NaHL^7	32	>256	<8	32	256	8
NaHL^8	32	256	8	8	256	32

that the antimycobacterial activity of complexes [Cu($\mathbf{L^1}$)-(H_2O)$_2$]–[Cu($\mathbf{L^8}$)(H_2O)$_2$], $\mathbf{NaHL^1}$–$\mathbf{NaHL^8}$ and their parent hydrazides also depend on the availability of iron suggests a similar mode of action. If this is the case, at least part of the observed antibacterial activity should be due to the parent hydrazides produced by dissociation of the Cu-complexes and hydrolysis of the hydrazone ligands inside the cell. In the case of [Cu($\mathbf{L^8}$)(H_2O)$_2$], the intracellularly released hydrazide would be a prodrug, which requires further hydrolysis to produce its active component, pyrazinoic acid. Interestingly, the parent hydrazides have lower antimycobacterial activities than the hydrazones $\mathbf{NaHL^1}$–$\mathbf{NaHL^8}$ (Table 3b) when added to the growth medium under the same conditions. These lower activities, however, do not necessarily correspond to lower intracellular potencies since the lower activities of the hydrazides could be due to restricted cellular uptake.

Since ferrous sulphate was used as the iron source in the activity tests, it is also conceivable that Fe(II) binds to $\mathbf{NaHL^1}$–$\mathbf{NaHL^8}$ or the parent hydrazides in the growth medium under high iron conditions, however, if the resulting iron complexes are formed, they are less potent than the corresponding Cu(II) complexes. The copper component of the complexes clearly exerts an additional inhibitory effect, as expected since copper is known to be highly toxic to *M. tuberculosis*.[26]

Finally, the pyruvate moiety may also be important due to its significance in the glyoxylate shunt cycle, a response of *M. tuberculosis* to nutrient starvation in the phagosome.[32] Amongst the known inhibitors of the glyoxylate shunt cycle in *E. coli* are the pyruvate compounds that activate the isocitrate dehydrogenase enzyme of the tricarboxylic acid (TCA) cycle and in turn inactivate the glyoxylate shunt pathway.[47]

Hydrolytic stability study

In order to investigate if the dissociation of the Cu(II) complexes accelerates the hydrolysis of the hydrazones to form their parent hydrazides, the stabilities of $\mathbf{NaHL^5}$ and [Cu($\mathbf{L^5}$)(H_2O)$_2$] in phosphate buffered saline (PBS) were compared. PBS is isotonic with human plasma and has previously been used in hydrolysis studies on related hydrazones.[48] Both compounds were dissolved in DMSO and the solutions diluted to a final concentration of 0.05 mM with PBS. The solutions (pH 7.4) were then maintained at 37 °C whilst the progress of hydrolysis was monitored spectrophotometrically at defined time-intervals.

Analysis of the UV-vis spectra obtained revealed the gradual hydrolysis and degradation of $\mathbf{NaHL^5}$ (Fig. 4). Hydrolysis was evidenced by a decrease in intensity of the absorption band at 270 nm, as expected for the formation of the parent hydrazide, the spectrum of which is shown for comparison (dotted line). Up to a time delay of 14 hours an isosbestic point is observed at 248 nm. However, an increase in absorbance at around 330 nm indicates further degradation or oxidation processes leading to the formation of additional species so that in spectra recorded between 53 and 120 hours after dissolution of $\mathbf{NaHL^5}$ an isosbestic point is no longer observed. In contrast, the overall shape of the UV-vis spectra recorded for [Cu($\mathbf{L^5}$)(H_2O)$_2$] changed very little. The slight decrease in intensity of the band at 325 nm can be explained by slow precipitation of some of the complex from the solution due to the limited water solubility of the compound. Consequently, Cu(II)-binding leads to a considerable stabilisation of the ligand towards hydrolysis.

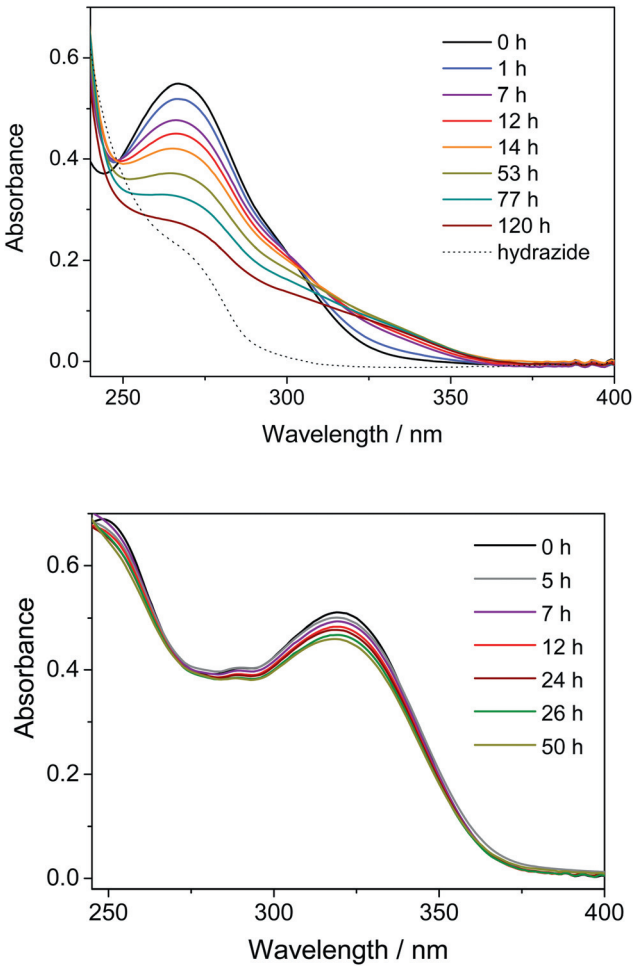

Fig. 4 Absorption spectra recorded in PBS buffer at pH 7.4 and 37 °C for $\mathbf{NaHL^5}$ in comparison with its parent hydrazide (top) and [Cu($\mathbf{L^5}$)-(H_2O)$_2$] (bottom), immediately after dissolution and after the indicated time-intervals given in hours.

Summary and conclusions

In summary, a series of eight pyruvate-based aroylhydrazones $\mathbf{HL^-}$ and their Cu(II)-complexes [Cu($\mathbf{L^n}$)(H_2O)$_2$] were synthesised, characterised and the crystal structures of two pyruvate-based aroylhydrazones and three Cu(II) complexes determined. Whilst the sodium salts of the eight pryruvate hydrazones were inactive, their neutral Cu(II) complexes exhibited promising antimycobacterial activities if tested under high iron conditions. As observed for INH, the activity of the complexes decreases significantly if the *M. tuberculosis* cells are grown under iron-deficient conditions. Consequently, the Cu(II) complexes may, at least partially, exhibit a similar mode of action, requiring dissociation, hydrolysis and activation of the released parent hydrazide by an iron-dependent peroxidase. A hydrolysis study performed with a representative ligand confirmed that the

dissociation of its Cu(II) complex leads to the hydrolysis of the hydrazone ligand to give its biologically active parent hydrazide. In case of the pyrazinamide-derivative $[Cu(\mathbf{L^8})(H_2O)_2]$, the released hydrazide could undergo further hydrolysis to produce the active component pyrazinoic acid.

Considering that pyrazinamide, which has a MIC value as high as 400 μg mL^{-1} under certain conditions,[49] is included in the current multi-drug regimen for the treatment of TB, complexes $[Cu(\mathbf{L^1})(H_2O)_2]$–$[Cu(\mathbf{L^8})(H_2O)_2]$ represent interesting potential prodrug candidates that merit further investigations.

Experimental

Materials and methods

The hydrazones and their Cu(II)-complexes were synthesised and characterised in the Chemistry Department, University of York. Chemicals were purchased from the following suppliers: sodium pyruvate (Fluka), hydrazides, pyrazine-2-carboxylate and $CuCl_2{\cdot}2H_2O$ (Sigma), analytical grade solvents (Fischer Scientific). Pyrazinoyl hydrazide was prepared according to a published procedure.[50] ^1H and ^{13}C NMR spectra were recorded on a Jeol ECS 400 instrument (^1H NMR 400 MHz, ^{13}C 100.6 MHz). Chemical shifts (δ) are given in ppm referenced to the residual DMSO solvent peak. Infrared spectra were recorded on an Avatar 370 FT-IR Thermo Nicolet instrument using KBr discs. ESI-MS spectra were recorded on a Bruker microTOF electrospray mass spectrometer. Melting points were obtained on a Stuart Scientific SMP3 melting point apparatus. Elemental analyses were performed on an Exeter analytical CE-440 elemental analyser.

General procedure for the preparation of pyruvate-based aroylhydrazones

The respective hydrazide (1.82 mmol) and sodium pyruvate (1.82 mmol) were dissolved in 25 mL of a water–methanol mixture (methanol–water; 7 : 3). The solution was heated under reflux for 2 hours. The product was precipitated with diethyl ether, isolated and recrystallised from ethanol. The purified product was dried *in vacuo*.

Preparation of sodium 2-[(4-methyl-benzoyl)-hydrazono]-propionate (NaHL^1). NaHL^1 was synthesised using 4-methyl benzoyl hydrazide 0.27 g (1.82 mmol) to give **NaHL^1**, 0.38 g (1.57 mmol, 86%), m.p.: 242–244 °C. Anal. calcd for $C_{11}H_{11}N_2O_3Na_1{\cdot}2.2H_2O$: C, 46.88; H, 5.51; N, 9.94. Found: C, 46.92; H, 5.41; N, 9.75. HR ESI-MS: Calcd for $C_{11}H_{12}N_2O_3Na_1$ ($[M + H]^+$) 243.0740, found: 243.0738, difference 0.3 mDa. ^1H NMR (DMSO-d_6, 400 MHz) δ: 2.36 (s, 3H, Ar–CH_3), 1.98 (s, 3H, CH_3), 7.31 (d, 2H, $J_{H–H}$ = 8.1 Hz Ar–H), 7.71 (d, 2H, $J_{H–H}$ = 8.1 Ar–H), 16.2 (1H, br, NH); ^{13}C NMR (DMSO-d_6, 100 MHz): 166.3, 161.9, 150.5, 141.7, 130.9, 129.3 127.0, 21.2, 21.0. Significant IR bands (KBr, ν cm^{-1}): 1649, 1631, 1610, 1575, 1476, 1368.

Preparation of sodium 2-[(4-nitro-benzoyl)-hydrazono]-propionate (NaHL^2). NaHL^2 was synthesised using 4-nitro-benzoyl hydrazide 0.33 g (1.82 mmol) to give **NaHL^2**, 0.47 g (1.72 mmol, 95%, m.p.: 204–205 °C. Anal. calcd for $C_{10}H_8N_3O_5Na_1{\cdot}2.2H_2O$: C, 38.40; H, 4.00; N, 13.28. Found: C, 38.69; H, 3.87; N, 13.43. HR ESI-MS: Calcd for $C_{10}H_9N_3O_5Na_1$ ($[M + H]^+$) 274.0434, found: 274.0429, difference: 0.5 mDa. ^1H NMR (DMSO-d_6, 400 MHz) 2.01 (s, 3H, CH_3), 8.03 (d, 2H, $J_{H–H}$ = 8.8 Ar–H), 7.55, 8.34 (d, 2H, $J_{H–H}$ = 8.8 Hz Ar–H), 16.7 (1H, br, NH); ^{13}C NMR (DMSO-d_6, 100.5 MHz): 166.1, 160.2, 151.9, 149.2, 139.6, 128.4, 124.0, 21.2. Significant IR bands (KBr, ν cm^{-1}): 1699, 1668, 1635, 1600, 1521, 1467, 1402, 1374, 1352.

Preparation of sodium 2-[(4-*tert*-butyl-benzoyl)-hydrazono]-propionate (NaHL^3). NaHL^3 was synthesised using 4-*tert*-butyl-benzoyl hydrazide 0.35 g (1.82 mmol) to give **NaHL^3**, 0.23 g (1.23 mmol, 67%), m.p.: 224–225 °C. Anal. calcd for $C_{14}H_{17}N_2O_3Na_1{\cdot}1.75H_2O$: C, 53.24; H, 6.54; N, 8.87. Found: C, 53.45; H, 6.41; N, 8.64. HR ESI-MS: Calcd for $C_{14}H_{19}N_2O_3$ ($[M - Na + 2H]^+$) 263.1390, found: 263.1391, difference: −0.1 mDa. ^1H NMR (DMSO-d_6, 400 MHz) 1.29 (s, 9H, Ar–C(CH_3)$_3$), 1.99 (s, 3H, CH_3), 7.74 (d, 2H, $J_{H–H}$ = 8.0 Hz Ar–H), 7.51 (d, 2H, $J_{H–H}$ = 8.0 Ar–H), 7.55 (m, 1H, Ar–H-8), 16.17 (1H, br, NH); ^{13}C NMR (DMSO-d_6, 100.5 MHz): 166.1, 161.7, 154.4, 150.4, 131.1, 126.7, 125.5, 34.6, 30.9, 21.2. Significant IR bands (KBr, ν cm^{-1}): 1652, 1634, 1610, 2963, 3426.

Preparation of sodium 2-[(3-methyl-4-nitro-benzoyl)-hydrazono]-propionate (NaHL^4). NaHL^4 was synthesised using 3-methyl-4-nitro-benzoyl hydrazide 0.35 g (1.82 mmol) to give **NaHL^4**, 0.43 g (1.5 mmol, 82%), m.p.: 243–245 °C. Anal. calcd for $C_{11}H_{10}N_3O_5Na_1{\cdot}0.25CH_3OH \times 1.8H_2O$: C, 40.95; H, 4.13; N, 12.45. Found: C, 41.24; H, 4.49; N, 12.82. HR ESI-MS: Calcd for $C_{11}H_{11}N_3O_5Na_1$ $[M + H]^+$ 288.0596, found: 288.0581, difference: 1.5 mDa. ^1H NMR (DMSO-d_6, 400 MHz) 2.01 (s, 3H, CH_3), 2.56 (s, 3H, Ar–CH_3), 7.78 (d,d, 1H, $J_{H–H}$ = 1.1, 8.4 Hz Ar–H), 7.87 (s, 1H, Ar–H), 8.09 (d, 1H, $J_{H–H}$ = 8.4 Hz Ar–H), 16.6 (1H, br, NH); ^{13}C NMR (DMSO-d_6, 100.5 MHz): 165.9, 160.1, 151.7, 150.5, 137.9, 133.2, 131.4, 125.5, 124.9, 21.1, 19.4. Significant IR bands (KBr, ν cm^{-1}): 1662, 1627, 1586, 1522, 1465, 1368, 1356.

Preparation of sodium 2-[(4-triflouromethyl-benzoyl)-hydrazono]-propionate (NaHL^5). NaHL^5 was synthesised using 4-triflouromethyl benzoyl hydrazide 0.37 g (1.82 mmol) to give **NaHL^5**, 0.48 g (1.62 mmol, 89%), m.p.: 125–128 °C. Anal. calcd for $C_{11}H_7N_2O_3F_3Na_2{\cdot}1.4CH_3OH \times 1.7H_2O$: C, 37.83; H, 4.10; N, 7.12. Found: C, 37.46; H, 3.73; N, 6.74. HR ESI-MS: Calcd for $C_{11}H_9N_2O_3F_3Na_1$ ($[M + H]^+$) 297.0457, found: 297.0465, difference: −0.7 mDa. ^1H NMR (DMSO-d_6, 400 MHz) 2.01 (s, 3H, CH_3), 7.89 (d, 2H, $J_{H–H}$ = 8.3 Hz Ar–H), 7.99 (d 2H, $J_{H–H}$ = 8.3 Hz, Ar–H) 16.6 (1H, br, NH); ^{13}C NMR (DMSO-d_6, 100.5 MHz): 165.9, 160.5, 151.6, 137.8, 131.5, 131.2, 127.8, 125.7, 125.2, 122.5, 21.1. Significant IR bands (KBr, ν cm^{-1}): 1635, 1632, 1580, 1525, 1472, 1367, 1331.

Preparation of sodium 2-[(3-fluoro-benzoyl)-hydrazono]-propionate (NaHL^6). NaHL^6 was synthesised using 3-fluoro-benzoyl hydrazide 0.27 g (1.82 mmol) to give **NaHL^6**, 0.36 g (1.46 mmol, 80%), m.p.: 254–257 °C. Anal. calcd for $C_{10}H_8N_2O_3FNa_1{\cdot}0.15CH_3OH \times 1.1H_2O$: C, 45.02; H, 4.02; N, 10.34. Found: C, 45.03; H, 3.92; N, 10.30. HR ESI-MS:

Calcd for $C_{10}H_9N_2O_3FNa_1$ ([M + H]$^+$) 247.0489, found: 247.0496, difference: −0.7 mDa. ^{1}H NMR (DMSO-d_6, 400 MHz) 1.99 (s, 3H, CH_3), 7.40–7.80 (m, 5H, Ar–H) 16.42 (1H, br, NH); ^{13}C NMR (DMSO-d_6, 100.5 MHz): 166.2, 163.4, 161.0, 160.6, 160.5, 151.2, 136.4, 136.3, 131.1, 131.0, 122.8, 122.8, 118.7, 118.5, 113.9, 113.7, 21.6. Significant IR bands (KBr, ν cm^{-1}): 1739, 1635, 1589, 1498, 1471, 1430, 1375, 1271.

Preparation of sodium 2-[(3-hydroxy-benzoyl)-hydrazono]-propionate (NaHL^7). **NaHL^7** was synthesised using 3-hydroxy-benzoyl hydrazide 0.27 g (1.82 mmol) to give **NaHL^7**, 0.39 g (1.59 mmol, 87%), m.p.: 278–281 °C. Anal. calcd for $C_{10}H_9N_2O_4Na_1{\cdot}1.6H_2O$: C, 44.00; H, 4.50; N, 10.26. Found: C, 44.16; H, 4.43; N, 10.10. HR ESI-MS: Calcd for $C_{10}H_{10}N_2O_4Na_1$ ([M + H]$^+$) 245.0533, found: 245.0533, difference: 0.0 mDa. ^{1}H NMR (DMSO-d_6, 400 MHz) 2.01 (s, 3H, CH_3), 6.97 (d,d, 1H, J_{H-H} = 2.08, 7.88, Ar–H), 7.78 (m 3H, Ar–H), 15.9 (1H, br, NH); ^{13}C NMR (DMSO-d_6, 100.5 MHz): 166.4, 162.3, 157.9, 150.5, 135.1, 129.8, 118.9, 117.3, 114.1, 21.2. Significant IR bands (KBr, ν cm^{-1}): 1663, 1633, 1612, 1585, 1457, 1373, 1296.

Preparation of sodium 2-[(pyrazine-2-carbonyl)-hydrazono]-propionate (NaHL^8). **NaHL^8** was synthesised using pyrazinoyl hydrazide 0.27 g (1.82 mmol) to give **NaHL^8** 0.36 g (1.46 mmol, 80%), m.p.: decomp. >200 °C. Anal. calcd for $C_8H_7N_4O_3Na_1{\cdot}0.15CH_3OH \times 1.75H_2O$: C, 36.73; H, 4.20; N, 21.02. Found: C, 36.55; H, 3.90; N, 20.76. HR ESI-MS: Calcd for $C_8H_9N_4O_3$ ([M − Na + 2H]$^+$) 209.0669, found: 209.0670, difference: −0.1 mDa. ^{1}H NMR (DMSO-d_6, 400 MHz) 2.02 (s, 3H, CH_3), 8.72 (d,d 1H, J_{H-H} = 2.5, 1.5 Hz Ar–H), 8.85 (d, 1H, J_{H-H} = 2.5 Ar–H), 9.21 (d, 1H, J_{H-H} = 1.4 Ar–H); ^{13}C NMR (DMSO-d_6, 100.5 MHz): 165.7, 159.1, 152.0, 147.6, 145.0, 143.9, 143.6, 21.4. Significant IR bands (KBr, ν cm^{-1}): 1670, 1625, 1573, 1486, 1430, 1385, 1275.

General procedure for the preparation of the copper complexes

To a methanolic solution of the respective pyruvate-based aroylhydrazone (0.58 mmol) was added $CuCl_2{\cdot}2H_2O$ (0.58 mmol). The mixture was stirred for 2 hours. The resultant clear green solution was allowed to evaporate slowly giving green coloured crystalline powder which was isolated, washed with water and redissolved in methanol. The resultant solution was allowed to evaporate slowly at room temperature, giving green coloured crystals, which were isolated and dried *in vacuo*.

Preparation of [Cu(L^1)(H$_2$O)$_2$]. [Cu(**L^1**)(H$_2$O)$_2$] was synthesised using **NaHL^1**, 0.14 g (0.58 mmol) and $CuCl_2{\cdot}2H_2O$, 0.10 g (0.58 mmol) to give [Cu(**L^1**)(H$_2$O)$_2$], 0.13 g (0.38 mmol, 65%), m.p.: 223–225 °C. Anal. calcd for $Cu_1C_{11}H_{14}N_2O_5{\cdot}0.3H_2O$: C, 40.88; H, 4.55; N, 8.67. Found: C, 40.54; H, 4.23; N, 8.48. ESI-MS: Calcd for $^{63}Cu_{(I)}{}_1C_{11}H_{15}N_2O_5Na_1$ ([M + H + Na]$^+$) 341.04, found: 341.02. Significant IR bands (KBr, ν cm^{-1}): 1622, 1482, 1377, 1363, 1318.

Preparation of [Cu(L^2)(H$_2$O)$_2$]. [Cu(**L^2**)(H$_2$O)$_2$] was synthesised using **NaHL^2**, 0.16 g (0.58 mmol) and $CuCl_2{\cdot}2H_2O$, 0.10 g (0.58 mmol) to give [Cu(**L^2**)(H$_2$O)$_2$], 0.08 g (0.24 mmol, 41%), m.p.: 250–252 °C. Anal. calcd for $Cu_1C_{10}H_{11}N_3O_7{\cdot}1.15H_2O$: C, 32.51; H, 3.63; N, 11.37. Found: C, 32.67; H, 3.31; N, 11.05. ESI-MS: Calcd for $^{63}Cu_{(I)}{}_1C_{10}H_{12}N_3O_7Na_1$ ([M + H + Na]$^+$) 371.99, found: 372.01. Significant IR bands (KBr, ν cm^{-1}): 1639, 1527, 1493, 1424, 1379, 1366, 1347, 1320.

Preparation of [Cu(L^3)(H$_2$O)$_2$]. [Cu(**L^3**)(H$_2$O)$_2$] was synthesised using **NaHL^3**, 0.16 g (0.58 mmol) and $CuCl_2{\cdot}2H_2O$ 0.1 g (0.58 mmol) to give [Cu(**L^3**)(H$_2$O)$_2$], 0.1 g (0.27 mmol, 47%), m.p.: 244–247 °C. Anal. calcd for $Cu_1C_{14}H_{18}N_2O_4{\cdot}0.25CH_3OH$: C, 48.92; H, 5.47; N, 8.01. Found: C, 49.09; H, 5.38; N, 7.87. ESI-MS: Calcd for $^{63}Cu_{(I)}{}_1C_{14}H_{19}N_2O_4Na_1$ ([M − H$_2$O + H + Na]$^+$) 365.05, found: 365.08. Significant IR bands (KBr, ν cm^1): 1651, 1635, 1609, 1575, 1558, 1476, 1436, 1385.

Preparation of [Cu(L^4)(H$_2$O)$_2$]. [Cu(**L^4**)(H$_2$O)$_2$] was synthesised using **NaHL^4**, 0.17 g (0.58 mmol) and $CuCl_2{\cdot}2H_2O$, 0.10 g (0.58 mmol) to give [Cu(**L^4**)(H$_2$O)$_2$], 120 mg (0.31 mmol, 54%), m.p.: 210–212 °C. Anal. calcd for $Cu_1C_{11}H_{13}N_3O_7{\cdot}0.1H_2O$: C, 36.06; H, 3.69; N, 11.47. Found: C, 36.06; H, 3.55; N, 11.35. ESI-MS: Calcd for $^{63}Cu_{(II)}{}_1C_{11}H_{12}N_3O_6Na_1$ ([M − H$_2$O + Na]$^+$) 368.00, found: 368.02. Significant IR bands (KBr, ν cm^{-1}): 1662, 1524, 1495, 1401, 1360, 1308.

Preparation of [Cu(L^5)(H$_2$O)$_2$]. [Cu(**L^5**)(H$_2$O)$_2$] was synthesised using **NaHL^5**, 0.17 g (0.58 mmol) and $CuCl_2{\cdot}2H_2O$ 0.1 g (0.58 mmol), to give [Cu(**L^5**)(H$_2$O)$_2$], 0.08 g (0.21 mmol, 36%), m.p.: 214–217 °C. Anal. calcd for $Cu_1C_{11}H_{11}N_2O_5F_3{\cdot}0.27H_2O$: C, 34.28; H, 3.27; N, 7.27. Found: C, 34.28; H, 3.07; N, 6.77. ESI-MS: Calcd for $^{63}Cu_{(I)}{}_1C_{11}H_{12}N_2O_5F_3Na_1$ ([M + H + Na]$^+$) 394.99, found: 395.01. Significant IR bands (KBr, ν cm^{-1}): 1640, 1626, 1491, 1379, 1365, 1323.

Preparation of [Cu(L^6)(H$_2$O)$_2$]. [Cu(**L^6**)(H$_2$O)$_2$] was synthesised using **NaHL^6**, 0.14 g (0.58 mmol) and $CuCl_2{\cdot}2H_2O$, 0.10 g (0.58 mmol) to give [Cu(**L^6**)(H$_2$O)$_2$], 0.06 g (0.19 mmol, 32%), m.p.: 232–235 °C. Anal. calcd for $Cu_1C_{10}H_{11}N_2O_5F_1{\cdot}0.27H_2O$: C, 45.02; H, 3.56; N, 8.57. Found: C, 45.03; H, 3.29; N, 8.25. ESI-MS: Calcd for $^{63}Cu_{(I)}{}_1C_{10}H_{12}N_2O_5F_1Na_1$ ([M + H + Na]$^+$) 344.99, found: 345.02. Significant IR bands (KBr, ν cm^{-1}): 1630, 1581, 1506, 1539, 1484, 1431, 1371, 1347.

Preparation of [Cu(L^7)(H$_2$O)$_2$]. [Cu(**L^7**)(H$_2$O)$_2$] was synthesised using **NaHL^7**, 0.14 g (0.58 mmol) and $CuCl_2{\cdot}2H_2O$ 0.1 g (0.58 mmol) to give [Cu(**L^7**)(H$_2$O)$_2$], 0.06 g (0.2 mmol, 34%), m.p.: 265–268 °C. Anal. calcd for $Cu_1C_{10}H_{12}N_2O_6$: C, 37.56; H, 3.78; N, 8.76. Found: C, 37.53; H, 3.85; N, 8.23. ESI-MS: Calcd for $^{63}Cu_{(I)}{}_1C_{10}H_{11}N_2O_5Na_1$ ([M − H$_2$O + H + Na]$^+$) 324.99, found: 325.01. Significant IR bands (KBr, ν cm^{-1}): 1645, 1588, 1498, 1458, 1376, 1364, 1347, 1302.

Preparation of [Cu(L^8)(H$_2$O)$_2$]. [Cu(**L^8**)(H$_2$O)$_2$] was synthesised using **NaHL^8**, 0.13 g (0.58 mmol) and $CuCl_2{\cdot}2H_2O$, 0.10 g (0.58 mmol) to give [Cu(**L^8**)(H$_2$O)$_2$], 0.11 g (0.36 mmol, 62%), m.p.: 137–139 °C. Anal. calcd for $Cu_1C_8H_{11}N_4O_5Cl \times 0.1\ CH_3OH$: C, 28.00; H, 3.17; N, 16.03. Found C, 27.81; H, 2.88; N, 15.78. ESI-MS: For $^{63}Cu_{(I)}{}_1C_8H_9N_4O_4Na_1$ ([M − H$_2$O + H + Na]$^+$), Calcd: 310.99, found: 311.03. Significant IR bands (KBr, ν cm^{-1}): 1640, 1614, 1578, 1535, 1471.

Hydrolytic stability study

Accurate weight measurements were conducted on a Mettler AE 240 five figure balance. 0.05 mM stock solutions of the ligands and Cu(II)-complexes in 90% phosphate buffered saline (PBS) and 10% spectrophotometric grade DMSO were prepared using calibrated Eppendorf pipettes. The solutions (pH 7.4) were then maintained at 37 °C whilst the progress of hydrolysis was monitored by recording absorption spectra at regular time intervals. The absorption spectra were recorded on an HP 8453 Agilent Diode Array spectrophotometer using a 5Q quartz UV cell with path length 10 mm.

X-Ray crystallography

Diffraction data for **NaHL^1**, [Cu(**L^1**)$(H_2O)_2$] and [Cu(**L^2**)-$(MeOH)_2$] were collected on a Bruker Smart Apex diffractometer with Mo-K_α radiation (λ = 0.71073 Å) using a SMART CCD camera. Absorption corrections were applied by SADABS (v2.10).[51] Structures were solved by direct methods using SHELXS-97 and refined by full-matrix least squares using SHELXL-97.[52] All non-hydrogen atoms were refined anisotropically. Hydrogen atoms were placed using a riding model and included in the refinement at calculated positions. Acidic protons were placed using difference map method.

Diffraction data for **H_2L^8** and [Cu(**L^4**)$(MeOH)_2$] were collected on an Oxford Diffraction SuperNova diffractometer with Mo-K_α radiation (λ = 0.71073 Å) using a EOS CCD camera. The crystals were cooled with an Oxford Instruments Cryojet. Face-indexed absorption corrections were applied using SCALE3 ABSPACK scaling. OLEX2[53] was used for overall structure solution, refinement and preparation of computer graphics and publication data. Within OLEX2, the algorithms used for structure solution were direct methods using SHELXS-97 and refinement by full-matrix least-squares used SHELXL-97[52] within OLEX2. All non-hydrogen atoms were refined anisotropically. Hydrogen atoms were placed using a riding model and included in the refinement at calculated positions. Acidic hydrogen atoms were placed using difference map method.

Crystal data and refinement details are summarised in Table S2.†

Screening of the compounds for antimycobacterial activity

The hydrazones and their Cu(II)-complexes were screened in the Department of Animal Sciences, School of Life Sciences, University of Hyderabad.

Mycobacterial strain and growth conditions

Mycobacterium tuberculosis ATCC 27294 was grown in Middlebrook 7H9 broth medium (pH 7.0, Difco, Detroit, MI, USA) containing 10% (v/v) albumin-dextrose-catalase (ADC; Difco) enrichment and 0.2% glycerol and maintained with shaking at 150 rpm at 37 °C.

Iron-regulated growth was performed in Proskauer and Beck medium (pH 6.8) with iron added at 0.02 μg Fe per mL (low iron) and 8 μg Fe per mL (high iron), respectively. Ferrous sulphate was used as the iron source. The iron-regulated cultures were harvested in the mid-log phase after 10 days of growth. The iron status of the organisms was confirmed by assaying the siderophores mycobactin and carboxymycobactin using established protocols.[25] Care was taken to ensure that the cells were harvested before the onset of iron limitation in high iron organisms. The cells were washed and re-suspended in the respective medium to get a cell density equivalent to McFarland 1 (3×10^8 cfu mL^{-1}) and further adjusted to get an OD_{600nm} of 0.15 (Biophotometer, Eppendorf, USA). This cell suspension was used for the screening of the compounds.

Preparation of the compounds for screening

Stock solutions of the compounds were prepared in HPLC grade dimethyl sulfoxide (Sigma Chemical Co., St. Louis, MO, USA) at a concentration of 10 mg mL^{-1}. These were filter-sterilized (0.22 μm filters, Sartorius) and stored at −80 °C.

Screening of the compounds

The compounds were first screened in the MB/BacT™ 240 Mycobacteria Detection System (BioMerieux/Organon Teknika, France) followed by the determination of the MIC values by Microplate Alamar Blue assay (MABA). Finally, the MIC values were confirmed in the MB/BacT™ 240 system by growth at MIC and sub-MIC concentrations of the compounds.

24 compounds, including the free ligands, their parent hydrazides and Cu-complexes were screened for antimycobacterial activity in the MB/BacT™240 Mycobacteria Detection System (BioMerieux/Organon Teknika, France). The detection system employs standard bottles of 10 mL of culture media to which 0.5 mL of the mycobacterial cell suspension (prepared as detailed above) was added. The system also included the 'proportion control' that was inoculated with 0.5 mL of the cell suspension diluted 1 : 100. The system was standardised for the screening by adding INH at 0.1–0.5 μg mL^{-1} final concentration. All the compounds were added at 256 μg mL^{-1} and checked for their effectiveness on *M. tuberculosis*.

This was carried out essentially as described earlier.[25] Briefly, it included testing of the compounds in 96 clear bottomed, sterile, microtitre plates (Corning, New York, USA). The outer perimeter wells were filled with 200 μL of sterile, distilled water to prevent evaporation from the experimental wells during incubation. 100 μL of 7H9 medium was added to all wells except those of column 2. 100 μL of the compound(s) to be tested was added to column 2. This represented the highest concentration of the compound(s). 100 μL of the compound(s) was added to column 3 followed by serial dilutions of the compounds from columns 3–10. Column 11 served as the control with no added drug. 100 μL of the cell suspension (1 : 50 dilution of the cell suspension prepared above) was added to all wells and the plate was incubated at 37 °C for 5 days. 50 μL of Alamar Blue [Invitrogen Corporation, Carlsbad, CA, USA; prepared as a 1 : 1 (v/v) mixture with 10% Tween-80 (Sigma)] was added to the first control well and observed after 12 h. If the colour changed from blue to pink, Alamar Blue was added to all the wells and visual

grading of the colour change was made 6 h after the dye addition. The MIC of the specific compound was taken as the lowest concentration in which there was no change of the blue colour of Alamar Blue indicating lack of any viable bacilli.

Once the MIC value was established by MABA, the MICs of the compounds were confirmed by adding them at MIC and sub-MIC concentrations in the MB/BacT™240 system.

Influence of iron levels on the antibacterial activity

The organisms were grown in high and low iron conditions as described above. The cells were harvested and re-suspended in the respective medium and tested by MABA, essentially as described above except that the 7H9 medium was replaced by high and low iron Proskauer and Beck medium.

Acknowledgements

A. J. and A. K. D. K. thank Dr Adrian Whitwood and Dr Robert Thatcher for help with the X-ray crystal structure determinations, Karl Heaton for recording ESI mass spectra and the Medical Research Council and the Holbeck Trust for supporting a Dorothy Hodgkin Post Graduate Award. P. D. and S. P. are thankful to Mr P. A. Inamdar and ISTRA for providing funds for this project. K. V. acknowledges the Department of Biotechnology (DBT) for a fellowship and M. S. thanks the Department of Science and Technology for financial assistance for the project and UGC-CAS for departmental funding.

References

1 World Health Organization, Fact sheet no. 104, 2010
2 E. C. Rivers and R. L. Mancera, *Drug Discovery Today*, 2008, **13**, 1090.
3 C. V. Smith, V. Sharma and J. C. Sacchettini, *Tuberculosis*, 2004, **84**, 45.
4 R. Maccari, R. Ottanà, F. Monforte and M. G. Vigorita, *Antimicrob. Agents Chemother.*, 2002, **46**, 294.
5 R. Maccari, R. Ottanà and M. G. Vigorita, *Bioorg. Med. Chem. Lett.*, 2005, **15**, 2509.
6 M. J. Hearn, M. H. Cynamon, M. F. Chen, R. Coppins, J. Davis, H. Joo-On Kang, A. Noble, B. Tu-Sekine, M. S. Terrot, D. Trombino, M. Thai, E. R. Webster and R. Wilson, *Eur. J. Med. Chem.*, 2009, **44**, 4169.
7 F. R. Pavan, P. I. da S. Maia, S. R. A. Leite, V. M. Deflon, A. A. Batista, D. N. Sato, S. G. Franzblau and C. Q. F. Leite, *Eur. J. Med. Chem.*, 2010, **45**, 1898.
8 N. Sinha, S. Jain, A. Tilekar, R. S. Upadhayaya, N. Kishore, G. H. Jana and S. K. Arora, *Bioorg. Med. Chem. Lett.*, 2005, **15**, 1573.
9 F. M. F. Vergara, C. H. S. Lima, M. G. M. O. Henriques, A. L. P. Candéa, M. C. S. Lourenço, M. L. Ferreira, C. R. Kaiser and M. V. N. de Souza, *Eur. J. Med. Chem.*, 2009, **44**, 4954.
10 D. Sriram, P. Yogeeswari and K. Madhu, *Bioorg. Med. Chem. Lett.*, 2006, **16**, 876.
11 M. J. Hearn and M. H. Cynamon, *J. Antimicrob. Chemother.*, 2004, **53**, 185.
12 M. Payton, R. Auty, R. Delgoda, M. Everett and E. Sim, *J. Bacteriol.*, 1999, **181**, 1343.
13 E. Sim, J. Sandy, D. Evangelopoulos, E. Fullam, S. Bhakta, I. Westwood, A. Krylova, N. Lack and M. Noble, *Curr. Drug Metab.*, 2008, **9**, 510.
14 B. Bottari, R. Maccari, F. Monforte, R. Ottanà, E. Rotondo and M. G. Vigorita, *Bioorg. Med. Chem. Lett.*, 2000, **10**, 657.
15 B. Bottari, R. Maccari, F. Monforte, R. Ottanà, E. Rotondo and M. G. Vigorita, *Bioorg. Med. Chem. Lett.*, 2001, **11**, 301.
16 R. Maccari, R. Ottanà, B. Bottari, E. Rotondo and M. G. Vigorita, *Bioorg. Med. Chem. Lett.*, 2004, **14**, 5731.
17 S. S. Kanwar, K. Lumba, S. K. Gupta, V. M. Katoch, P. Singh, A. K. Mishra and S. B. Kalia, *Biotechnol. Lett.*, 2007, **30**, 677.
18 P. Krishnamoorthy, P. Sathyadevi, K. Senthilkumar, P. T. Muthiah, R. Ramesh and N. Dharmaraj, *Inorg. Chem. Commun.*, 2011, **14**, 1318.
19 A. Ray, S. Banerjee, S. Sen, R. Butcher, G. Rosair, M. Garland and S. Mitra, *Struct. Chem.*, 2007, **19**, 209.
20 J. D. Ranford, J. J. Vittal and Y. M. Wang, *Inorg. Chem.*, 1998, **37**, 1226.
21 P. V. Bernhardt, *Dalton Trans.*, 2007, 3214.
22 N. L. Wengenack, H. M. Hoard and F. Rusnak, *J. Am. Chem. Soc.*, 1999, **121**, 9748.
23 A. Milano, F. Forti, C. Sala, G. Riccardi and D. Ghisotti, *J. Bacteriol.*, 2001, **183**, 6801.
24 V. C. Yeruva, C. A. S. S. Sundaram and M. Sritharan, *Ind. J. Biochem. Biophys.*, 2005, **42**, 34.
25 M. Sritharan, V. C. Yeruva, S. C. Sivasailappan and S. Duggirala, *World J. Microbiol. Biotechnol.*, 2006, **22**, 1357.
26 F. Wolschendorf, D. Ackart, T. B. Shrestha, L. Hascall-Dove, S. Nolan, G. Lamichhane, Y. Wang, S. H. Bossmann, R. J. Basaraba and M. Niederweis, *Proc. Natl. Acad. Sci. U. S. A.*, 2011, **108**, 1621.
27 B. Koçyiğit-Kaymakçioğlu, E. Oruç, S. Unsalan, F. Kandemirli, N. Shvets, S. Rollas and A. Dimoglo, *Eur. J. Med. Chem.*, 2006, **41**, 1253.
28 B. Koçyiğit-Kaymakçioğlu, E. E. Oruç-Emre, S. Unsalan and S. Rollas, *Med. Chem. Res.*, 2008, **18**, 277.
29 R. Rawat, A. Whitty and P. J. Tonge, *Proc. Natl. Acad. Sci. U. S. A.*, 2003, **100**, 13881.
30 W. Shi, X. Zhang, X. Jiang, H. Yuan, J. S. Lee, C. E. Barry, H. Wang, W. Zhang and Y. Zhang, *Science*, 2011, **333**, 1630.
31 D. Shingnapurkar, P. Dandawate, C. E. Anson, A. K. Powell, Z. Afrasiabi, E. Sinn, S. Pandit, K. V. Swamy, S. Franzblau and S. Padhye, *Bioorg. Med. Chem. Lett.*, 2012, **22**, 3172.
32 J. D. McKinney, K. H. zu Bentrup, E. J. Munoz-Elías, A. Miczak, B. Chen, W.-T. Chan, D. Swenson, J. C. Sacchettini, W. R. Jacobs and D. G. Russell, *Nature*, 2000, **406**, 735.
33 G. Palla, G. Predieri, P. Domiano, C. Vignali and W. Turner, *Tetrahedron*, 1986, **42**, 3649.
34 E. A. Enyedy, M. F. Primik, C. R. Kowol, V. B. Arion, T. Kiss and B. K. Keppler, *Dalton Trans.*, 2011, **40**, 5895.
35 P. V. Bernhardt, M. Martinez, C. Rodriguez and M. Vazquez, *Dalton Trans.*, 2012, **41**, 2122.
36 F. H. Allen, O. Kennard, D. G. Watson, L. Brammer, A. G. Orpen and R. Taylor, *J. Chem. Soc., Perkin Trans. 2*, 1987, S1.
37 W.-T. Wu, S.-Y. He, F. Liu, F.-Y. Chen, Y.-Y. Wang and Q.-Z. Shi, *J. Coord. Chem.*, 2008, **61**, 2703.
38 H. W. Wong, K. M. Lo and S. W. Ng, *Acta Crystallogr., Sect. E: Struct. Rep. Online*, 2009, **65**, o419.
39 H. W. Wong, K. M. Lo and S. W. Ng, *Acta Crystallogr., Sect. E: Struct. Rep. Online*, 2009, **65**, o816.
40 H. Friebolin, *Ein-und zweidimensionale NMR-Spektroskopie*, VCH, Weinheim, 1988, p. 49.
41 P.V. Bernhardt, P. Chin, P. C. Sharpe and D. R. Richardson, *Dalton Trans.*, 2007, 3232.
42 L. Gianelli, V. Amendola, L. Fabbrizzi, P. Pallavicini and G. G. Mellerio, *Rapid Commun. Mass Spectrom.*, 2001, **15**, 2347.
43 A. W. Addison, T. N. Rao, J. Reedijk, J. van Rijn and G. C. Verschoor, *J. Chem. Soc., Dalton Trans.*, 1984, 1349.
44 F. Liu, W.-T. Wu, W.-P. Zhang, F.-Y. Chen and S.-Y. He, *Acta Crystallogr., Sect. E: Struct. Rep. Online*, 2007, **63**, m2450.
45 A. E. Martell and R. M. Smith, *Critical Stability Constants*, Plenum Press, NY, vol. 3, 1977, p. 66.
46 H. A. Shoeb, B. U. Bowman Jr., A. C. Ottolenghi and A. J. Merola, *Antimicrob. Agents Chemother.*, 1985, **27**, 404.
47 E. M. T. El-Mansi, H. G. Nimmo and W. H. Holms, *J. Gen. Microbiol.*, 1986, **132**, 797.
48 J. L. Buss and P. Ponka, *Biochim. Biophys. Acta, Gen. Subj.*, 2003, **1619**, 177.
49 M. Salfinger and L. Heifets, *Antimicrob. Agents Chemother.*, 1988, **32**, 1002.
50 M. Abdel-Aziz and H. M. Abdel-Rahman, *Eur. J. Med. Chem.*, 2010, **45**, 3384.
51 G. M. Sheldrick, *SADABS (v2.10)*, Bruker AXS Inc., Madison, Wisconsin, USA, 2007.
52 G. M. Sheldrick, *SHELXL-97*, University of Göttingen, Germany, 1997.
53 O. V. Dolomanov, L. J. Bourhis, R. J. Gildea, J. A. K. Howard and H. Puschmann, *J. Appl. Crystallogr.*, 2009, **42**, 339.